Conformational Flexibility of the Benzyl-Guanine Adduct in a Bypass Polymerase Active Site Permits Replication: Insights from Molecular Dynamics Simulations

Katie A. Wilson and Stacey D. Wetmore*

Department of Chemistry and Biochemistry, University of Lethbridge, 4401 University Drive West, Lethbridge, Alberta, Canada T1K 3M4
* Tel.: 403-329-2323. Fax: 403-329-2057. E-mail: stacey.wetmore@uleth.ca. ORCID: 0000-0002-5801-3942

Supplementary Information

Dpo4 Crystal Structures Considered in the Present Work

5EWD, 1S0M, 1S0O, 2AGQ, 2ASD, 2ATL, 2C22, 2J6S, 2J6T, 2R8I, 2UVR, 2UVU, 2UVV, 2UVW, 2V4Q, 2V4R, 2W8L, 2W9A, 2XCP, 3GII, 3GIJ, 3GIK, 3GIM, 3KHL, 3KHR, 3QZ7, 3QZ8, 3RAQ, 3RAX, 3RB3, 3RB4, 3RB6, 3RBD, 3RBE, 3T5H, 3T5J, 3T5K, 3T5L, 3V6H, 3V6J, 4JUZ, 4JV0, 4JV1, 4JV2, 4QW8, 4QWB

Table S1. Average structural parameters with standard deviations during MD simulations on the preinsertion or dCTP insertion complex for the replication of dG or Bz-dG by Dpo4.

	dG	dG:dCTP	*anti*-Bz-dG	*syn*-Bz-dG	*anti*-Bz-dG:dCTP	*syn*-Bz-dG:dCTP
rmsd	1.641±0.353 Å	1.131±0.145 Å	1.578±0.236 Å	1.284±0.201 Å	1.178±0.122 Å	1.249±0.188 Å
dG* χ[a]	236.1±22.0°	255.5±12.9 °	246.4±15.1°	42.0±15.7°	267.2±13.7°	29.3±14.8°
dG* pucker	C2′-*endo*	C2′-*endo*	C2′-*endo*	C1′–*exo*	C2′-*endo*	C1′–*exo*
Bz-dG* θ[a]	NA[b]	NA[b]	149.9±52.3°	1.2±50.1°	106.5±116.1°	294.9±86.0°
Bz-dG* ϕ[a]	NA[b]	NA[b]	177.9±12.7°	179.0±9.8°	177.0±10.2°	178.8±10.4°
Bz-dG* ξ[a]	NA[b]	NA[b]	3.9±97.9°	355.0±58.3°	316.4±92.5°	50.0±87.3°
dCTP χ[a]	NA[b]	225.5±10.1°	NA[b]	NA[b]	232.3±16.2°	255.6±14.8°
dCTP pucker	NA[b]	C1′–*exo*	NA[b]	NA[b]	C1′–*exo*	C1′–*exo*
dG*:dCTP d(C1′–C1′)	NA[b]	10.773±0.138 Å	NA[b]	NA[b]	11.371±0.319 Å	11.082±0.263 Å

[a]dG* = dG or Bz-dG. See Figure 1 for the definitions of key nucleoside dihedral angles. [b]Not applicable.

Table S2. Average and standard deviations for stacking interactions (kcal/mol) between the dG*:dCTP and 3′–dC:dG pairs, and dG* and 5′–dC (dG * = dG or Bz-dG) during MD simulations on the Dpo4 preinsertion and insertion complexes.

	dG	dG:dCTP[a]	*anti*-Bz-dG	*syn*-Bz-dG	*anti*-Bz-dG:dCTP[a]	*syn*-Bz-dG:dCTP[a]
dG*:5'–dC	–0.5±0.5	–0.3±0.1	–0.3±0.4	–1.2±0.4	–2.3±1.3	–1.3±0.4
dG*:3'–dC	–6.1±0.9	–6.7±0.7	–7.1±0.8	–7.2±0.6	–6.8±0.9	–5.9±0.7
dG*:3'–dG	–0.9±0.5	–2.0±0.5	–6.2±1.0	–6.4±0.9	–2.0±0.6	–3.7±0.9
dCTP:3'–dC	NA[b]	–6.0±0.6	NA[b]	NA[b]	–5.0±1.0	–3.1±0.9
dCTP:3'–dG	NA[b]	–0.7±0.2	NA[b]	NA[b]	–1.0±0.5	–1.5±0.7

[a]Strength of the (AMBER) stacking between dG or Bz-dG and the indicated flanking base. [b]Not applicable.

Table S3. Occupancies (percentage of simulation time), average C1′–C1′ distance with standard deviation (Å), and average hydrogen-bond strength with standard deviation (kcal/mol) for the 3′–dC:dG pair with respect to dG or Bz-dG during MD simulations on the corresponding Dpo4 preinsertion and insertion complexes.

	dG(O6)···dC(HN4)[a]	dG(N1H)···dC(N3)[a]	dG(N2H)···dC(O2)[a]	d(C1′–C1′)	3′ Base Pair Hydrogen Bond[b]
dG	99%	100%	100%	10.740±0.163 Å	–28.1±2.8
dG:dCTP	99%	100%	100%	10.728±0.158 Å	–28.9±2.6
anti-Bz-dG	97%	98%	100%	10.619±0.186 Å	–27.6±3.0
syn-Bz-dG	98%	100%	100%	10.708±0.171 Å	–28.2±2.8
anti-Bz-dG:dCTP	92%	99%	100%	10.606±0.188 Å	–27.7±3.3
syn-Bz-dG:dCTP	100%	100%	100%	10.740±0.155 Å	–29.0±2.5

[a]Hydrogen-bonding occupancies are based on a distance cutoff of < 3.4 Å and an angle cutoff of > 120°. [b]Strength of the (AMBER) hydrogen bond in the base pair 3′ with respect to dG or Bz-dG.

Table S4. Average reaction parameters with standard deviations during MD simulations on the dCTP insertion complex for the replication of dG or Bz-dG by Dpo4.

	Reaction Distance[a]	Reaction Angle[b]	Coordination Catalytic Mg^{2+}[c]	Coordination Binding Mg^{2+}[c]
dG:dCTP	3.529±0.158 Å	168.8±5.8°	6/6	5/6 (PβO)
anti-Bz-dG:dCTP	3.477±0.152 Å	168.4±5.9°	6/6	5/6 (PβO)
syn-Bz-dG:dCTP	3.425±0.217 Å	168.9±5.7°	6/6	5/6 (PβO)

[a]Pα···O3′ distance. [b]∠(PαβPαO3′) angle. [c]Number of coordinated atoms within < 2.5 Å for < 90% of the simulation/Number of possible coordinated atoms, with atom not coordinated to Mg^{2+} throughout the simulation indicated in parentheses. See Figure S2 for coordination of Mg^{2+} ions.

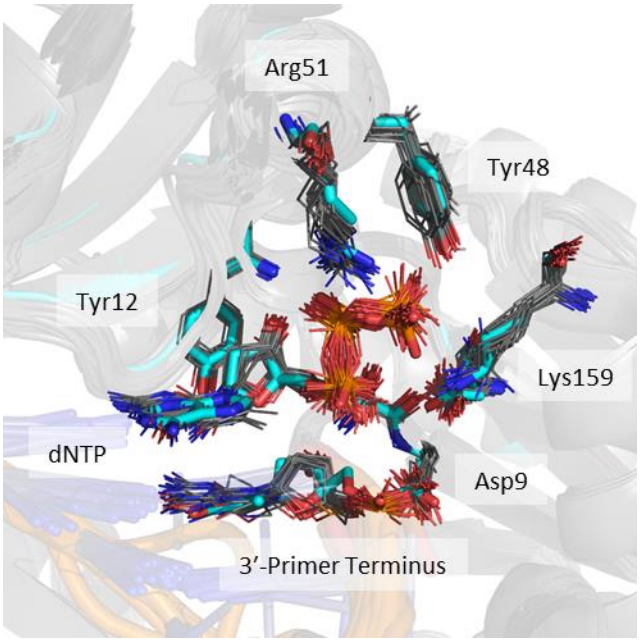

Figure S1. Overlay of the active site region of 45 crystal structures of Dpo4 ternary complexes obtained under a variety of crystallization conditions. The active site from 1S0M, which was used as the starting point for the present work, is highlighted in cyan.

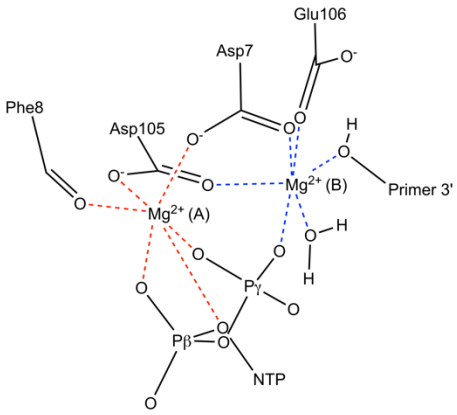

Figure S2. Coordination of the dNTP binding [Mg^{2+} (A)] and catalytic [Mg^{2+} (B)] Mg^{2+} ions.

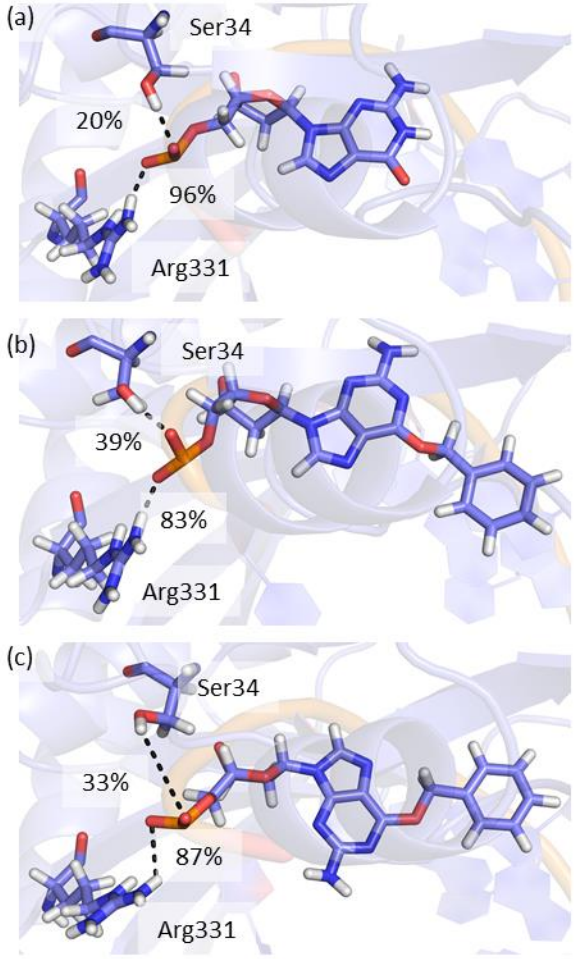

Figure S3. Representative MD structures of the (a) dG, (b) *anti*-Bz-dG, and (c) *syn*-Bz-dG preinsertion complexes for replication by Dpo4 depicting the interactions between the template base and surrounding amino acids.

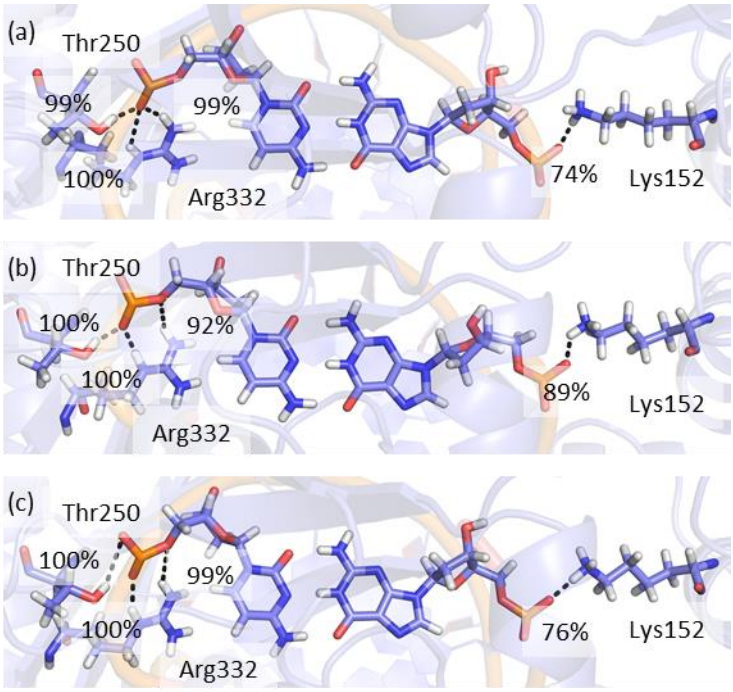

Figure S4. Representative MD structures of the (a) dG, (b) *anti*-Bz-dG, and (c) *syn*-Bz-dG preinsertion complexes for replication by Dpo4 depicting the interactions between the 3'–dC:dG base pair and surrounding amino acids.

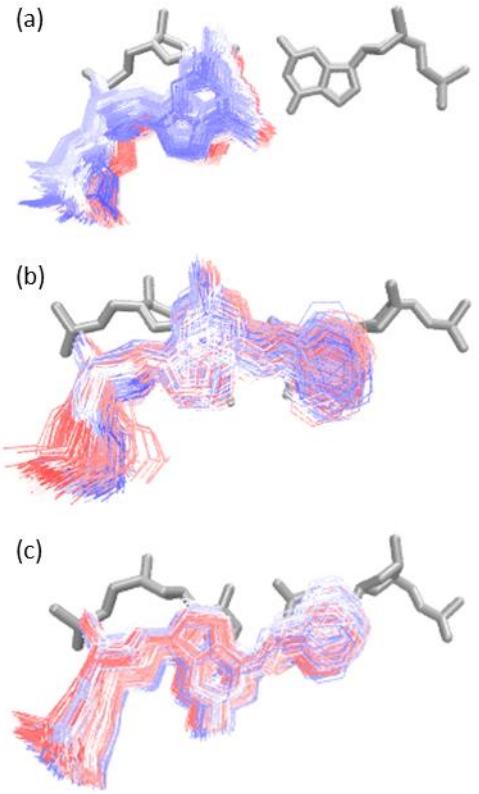

Figure S5. Overlay of orientations adopted throughout the MD simulation with the simulation time indicated in color (red [0 ns] to white [50 ns] to blue [100 ns]) for the (a) dG, (b) *anti*-Bz-dG, and (c) *syn*-Bz-dG preinsertion complexes for replication by Dpo4. Only the 3'–dC:dG pair is shown for simplicity.